

Study of the Influence of the Angle Between the Bottom Blowing Elements on the Dynamic Conditions in a 300t Converter



Liuji Yao, Rong Zhu, Huixiang Yu, Kai Dong, Qiang Feng and Yixing Tang

Abstract In this paper, the converter steelmaking process is studied using numerical simulations and hydraulic model experiments, in order to examine the influence of the angle between the bottom blowing elements and the gas flow rate, on the flow characteristics of the molten pool. A 300t converter is used. The results demonstrated that the mixing time and velocity field distribution, of the molten pool, changed with the angle between the bottom blowing nozzles. Increasing the bottom blowing gas flow rate improved the dynamic conditions of the bath, accelerating the mass transfer process and reducing the volume fraction of the dead zone. Two arrangements with angles of 90° and 105° were applied to two furnace regimes. The industrial experiments showed that a large angle between the nozzles was favorable because it accelerated the decarburization and dephosphorization. This reduced the endpoint carbon–oxygen equilibrium of molten steel and reduced the content of iron oxide and TFe in the endpoint slag.

Keywords 300t converter · Hydraulic model · Numerical simulation · Angle between the elements

Introduction

The converter steelmaking process is complex, involving thermodynamics and dynamics. Factors involved include a top-blown supersonic jet, the movement of the bottom blow stream, the flow of molten steel, and slag and the mass transfer

L. Yao · R. Zhu (✉) · H. Yu · K. Dong · Q. Feng · Y. Tang
School of Metallurgical and Ecological Engineering, University of Science and Technology
Beijing, Beijing 100083, China
e-mail: zhurong1_1201@126.com

H. Yu
e-mail: 821881796@qq.com

Beijing Key Laboratory of Research Center of Special Melting and Preparation of High-End Metal Materials, University of Science and Technology Beijing, Beijing 100083, China

© The Minerals, Metals & Materials Society 2020
Z. Peng et al. (eds.), *11th International Symposium on High-Temperature Metallurgical Processing*, The Minerals, Metals & Materials Series,
https://doi.org/10.1007/978-3-030-36540-0_31

process between the molten steel and slag. Among these factors, the bottom blow stream has the greatest influence on the dynamics.

Since the middle of the twentieth century, with the development of numerical simulation technology, researchers have carried out many studies of the fluid dynamics in the process of converter steelmaking and used hydraulic simulation results to verify these tests [1–4]. Lou et al. [5] used numerical simulations and hydraulic experiments to analyze the dynamics of the pool in the converter. They considered that when the bottom blowing component is distributed in the range of 0.3–0.4 D (D is the diameter of the converter furnace), the bottom blowing stream has the greatest stirring effect on the molten pool. Liu et al. [6] established a three-dimensional model for the converter, and carried out numerical simulations and hydraulic experiments of different schemes. They determined a mixing law for the bottom blowing stream on the molten metal pool. Caffery [7] established a model for energy exchange in molten metal pools and deduced that the bottom blow stream is beneficial to the uniform distribution of bath temperature. Ramirez [8] conducted a numerical simulation study on the electric arc furnace to investigate the flow characteristics of the molten metal pool. Gu et al. [9] used an Euler-Lagrangian model to perform a two-phase flow, numerical simulation study of a steelmaking process, with two bottom blowing elements.

In summary, research on the bottom blowing process of the converter has always been an important topic. Therefore, in this paper we look at a 300t converter, and adjust the influence of the bottom blowing stream on the dynamic characteristics of the molten pool, by adjusting the angle between the bottom blowing elements.

Mathematical Modeling

In this study, a three-dimensional full-scale mathematical model is established for a 300t converter. The numerical simulation process used the volume of fluid (VOF) [10] approach, to investigate the effect of the bottom blowing gas on the dynamics of molten steel, while altering the angles of the elements.

A. Assumptions

The assumption is specific: (1) The bottom blowing gas (argon and compressed air) and liquid (steel and water) are non-isothermal fluids. (2) The bottom blowing gas is a compressible Newtonian fluid, and the molten steel is an incompressible Newtonian fluid. (3) Chemical reactions in the pool are ignored. (4) The wall of the converter is nonslip, and the velocity near the wall is calculated according to the standard wall Eq. (5) The viscosity of each fluid phase and the surface tension between the phases are considered to be constant.

B. VOF Modeling

The VOF model is a multi-phase model, that is commonly used for numerical simulations of steelmaking. For the i th phase, the continuity equation is as follows,

$$\frac{\partial \alpha_i}{\partial t} + \vec{v}_i \cdot \nabla \alpha_i = \frac{S_{\alpha_i}}{\rho_i} + \frac{1}{\rho_i} \sum_{i=1}^n (\dot{m}_{ij} - \dot{m}_{ji}) \tag{1}$$

where \vec{v}_i is the speed in the direction i , ms^{-1} , \dot{m}_{ij} is the mass transfer from phase i to phase j , kg , and \dot{m}_{ji} is the mass transfer from phase j to phase i , kg . S_{α_i} is the source term, which is zero. The sum of the volume fractions of the phases in the calculation process is 1 as shown in the following equation.

$$\sum_{i=1}^n \alpha_i = 1 \tag{2}$$

All variable properties that appeared in the transport equation were determined for each phase, the equations are expressed as

$$\rho = \sum_{i=1}^n \alpha_i \rho_i \quad \mu = \sum_{i=1}^n \alpha_i \mu_i \tag{3}$$

where ρ is the average density of fluid, kg m^{-3} , ρ_i is the density of i th phase, kg m^{-3} , and the gas satisfied the ideal gas equation, i.e. $p = \rho RT$, and the density of the liquid was considered to be constant; μ is average viscosity of volume fraction, $\text{kg m}^{-1} \text{s}^{-1}$, μ_i is the viscosity of i th phase, $\text{kg m}^{-1} \text{s}^{-1}$.

In the VOF model, the momentum equation was given in Eq. 5.

$$\frac{\partial}{\partial t} (\rho \vec{v}) + \nabla \cdot (\rho \vec{v} \vec{v}) = -\nabla p + \nabla \cdot [\mu (\nabla \vec{v} + \nabla \vec{v}^T)] + \rho \vec{g} + \vec{F} \tag{4}$$

where ρ and μ are given in Eqs. (3) and (4); \vec{v} is the instantaneous velocity of phase, m s^{-1} ; p is static pressure, Mpa ; \vec{g} is the force of gravity, N ; \vec{F} is volume force, N .

In the VOF model, the surface tension is regarded as a volume force, and the continuum surface force model is used, this is expressed as follows,

$$f_\sigma = \int_V \sigma \kappa \cdot \nabla \alpha dV = \sigma \kappa_i \cdot (\nabla \alpha_i) V_i \tag{5}$$

where σ is surface tension coefficient, N m^{-1} , in this paper the value of σ is 1.5 N m^{-1} ; κ is surface curvature, constrained by the equation $\kappa_i = -\left[\nabla \cdot \left(\frac{\nabla \alpha}{|\nabla \alpha|} \right) \right]_i$

C. Energy Model

The energy equation is shared among the phases, this is shown in the following expression.

$$\frac{\partial}{\partial t} (\rho E) + \nabla \cdot (\vec{v} (\rho E + p)) = \nabla \cdot (k_{eff} \nabla T) + S_h \tag{6}$$

D. Turbulence Modeling

In this paper, the turbulence model used is a standard k-ε turbulence model. The expression of the turbulence kinetic energy, k, and rate of dissipation, ε, are as follows,

$$\frac{\partial}{\partial t}(\rho k) + \frac{\delta}{\delta x_i}(\rho k u_i) = \frac{\delta}{\delta x_j} \left[\left(\mu + \frac{\mu_t}{\sigma_k} \right) \frac{\delta k}{\delta x_j} \right] + G_k + G_b - \rho \varepsilon - Y_M + S_k \tag{7}$$

$$\frac{\partial}{\partial t}(\rho \varepsilon) + \frac{\delta}{\delta x_i}(\rho \varepsilon u_i) = \frac{\delta}{\delta x_j} \left[\left(\mu + \frac{\mu_t}{\sigma_\varepsilon} \right) \frac{\delta \varepsilon}{\delta x_j} \right] + C_{1\varepsilon} \frac{\varepsilon}{k} (G_k + C_{3\varepsilon} G_b) - C_{2\varepsilon} \rho \frac{\varepsilon^2}{k} + S_\varepsilon \tag{8}$$

where $C_{1\varepsilon}$, $C_{2\varepsilon}$, and $C_{3\varepsilon}$ are constants [11], σ_k and σ_ε are the turbulent Prandtl numbers for k and ε, respectively. S_k and S_ε are user-defined source terms, that are set to zero for this study.

E. Computation Methodology

In this study, the influence on the molten pool dynamic characteristics, from the angles between the four bottom blowing elements, was examined. This was done for a 300t converter, using numerical and water simulations. The experimental scheme is shown in Table 1.

In order to ensure the accuracy and effectiveness of the numerical simulation results, three-dimensional full-scale modeling of the 300t converter was carried out. Figure 1 is a schematic diagram of the converter geometry model and the bottom blowing nozzle arrangement, Table 2 shows the specific values of the geometrical parameters. Spatial discreteness is an unobtainable step in the numerical simulation,

Table 1 Parameters used in the present simulation and experiments

Scheme	γ (°)	δ (°)	Bottom blowing flow rate (Nm ³ /h)	
			Prototype	Hydraulics experiment
1	22.5	22.5	600/800/1000	1.61/2.15/2.68
2	30	30	600/800/1000	1.61/2.15/2.68
3	45	45	600/800/1000	1.61/2.15/2.68
4	60	45	600/800/1000	1.61/2.15/2.68

Fig. 1 Geometric representations of the converter and the bottom blowing nozzles arrangement

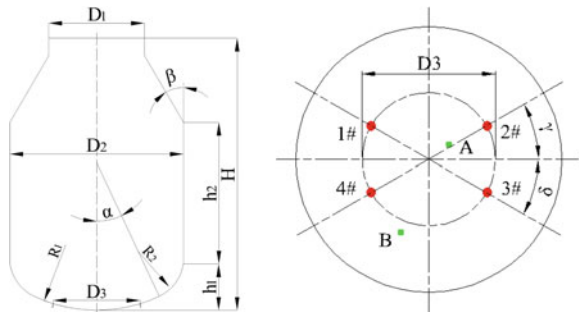


Table 2 Parameters used in the present simulation and experiments

Items	Converter prototype	Water model
Converter capacity (ton)	300	–
D1 (mm)	3600	514.3
D2 (mm)	6532	933.1
H (mm)	10257	1465.3
h1 (mm)	1748	249.7
h2 (mm)	5328	761.1
α (°)	25	25
β (°)	30	30
R1 (mm)	5567	795.3
R2 (mm)	1618	231.1
Bottom blowing arrangement diameter, D3 (mm)	3266	466.6
Bottom nozzle hydraulic diameter, d (mm)	8.3	1.2
Molten bath depth, h (mm)	1844	263.4
Bottom blowing flow rate (Nm ³ /h)	600/800/1000	1.61/2.15/2.68

as shown in Fig. 2. In order to verify the number of grids that is most suitable for the calculation model used in this paper, the area-weighted average velocity of the molten bath was monitored under the conditions of a coarse mesh (423759), a fine mesh (612896), and a medium mesh (562685). Figure 3 is the average velocity curve for the monitoring surface, with respect to the calculation time. The results showed that the average velocity for the fine mesh and the medium mesh surface differed by 1.5%, and the average velocity of the medium mesh and the coarse mesh surface differed by 4.6%. Therefore, in the subsequent numerical simulations, medium grids are used.

The choice of boundary conditions in the numerical simulation calculation process is especially important for the accuracy of the results and the stability of the

Fig. 2 Detailed grid arrangements of numerical simulation model (scheme 4)

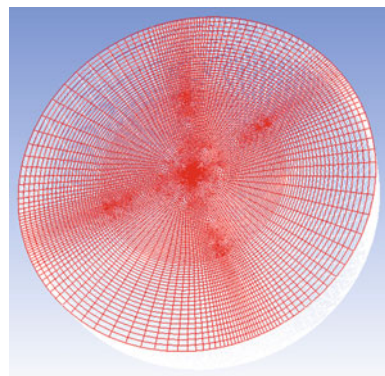
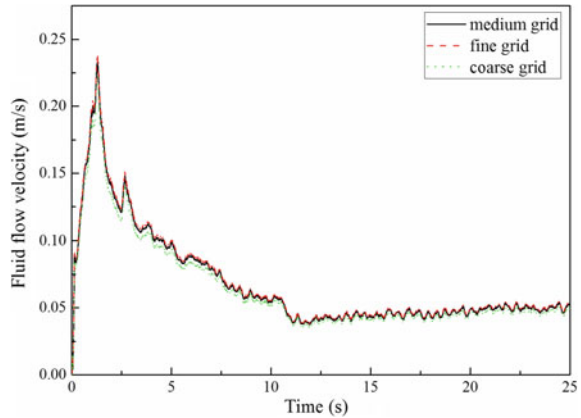


Fig. 3 Fluid flow velocity of the molten bath under three grid levels (scheme 4)



calculation. The inlet boundary condition of bottom blowing elements was a mass flow inlet, and the inlet pressure was set at 2.0×10^5 Pa. The outlet boundary condition was a pressure outlet, and the pressure was set at 1.10×10^5 Pa. For the walls, a nonslip condition was used and the standard wall function was adopted.

During the numerical simulation process, the first-order implicit transient method, using a pressure-based solver, was applied. The pressure-velocity coupling scheme was achieved using the PISO algorithm, the pressure discrete format used PRESTO!, and the interpolation scheme used a Geo-Reconstruct method. A second-order upwind scheme was applied to the momentum equations and a first-order upwind scheme was applied to the turbulent kinetic energy equation and turbulent dissipation rate equation. In this paper, when the energy residuals were less than 1×10^{-6} , and the residuals of other variables were less than 1×10^{-3} , the calculation process was considered to have reached convergence. The numerical simulation process used a time step of 1×10^{-5} s.

Hydraulics Experiment and Computational Verification

A. Hydraulics Experiment

The model scale used for the hydraulics experiment was 1/7, and the mold was made of plexiglass. The water model experimental apparatus are shown in Fig. 4. Table 3 shows the physical properties of the fluid used in this study.

During the steel making process, bubbles are mainly subject to inertial forces and gravity. In order to satisfy the dynamic similarity, the Froude number of the water

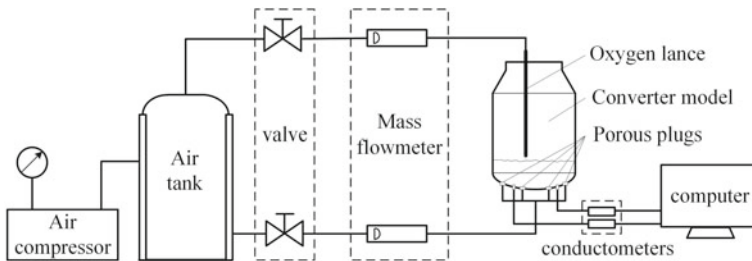


Fig. 4 Experimental instruments of water model experiment

Table 3 Physical properties of fluid

Item	Steel	Water	Argon	Air
Density, kg/m ³	7200	1000	1.63	1.225
Viscosity, kg/m/s	6.4 × 10 ⁻³	0.001	2.125 × 10 ⁻⁵	1.789 × 10 ⁻⁵
Surface Tension, N/m	1.5	0.071	–	–
Thermal conductivity, W/m/K	15	0.6	0.0158	0.0242
Specific heat, J/kg/K	670	4182	520.64	1006.43
Temperature, K	1873	300	300	300

model must be equal to the Froude number of the prototype. The equations are as follows,

$$Fr'_w = Fr'_p \quad (9)$$

$$\frac{Q_w^2}{gL_w(n \cdot \frac{\pi}{4} \cdot L_w^2 \cdot 3600)^2} \cdot \frac{\rho_{gw}}{\rho_{lw} - \rho_{gw}} = \frac{Q_p^2}{gL_p(n \cdot \frac{\pi}{4} \cdot L_p^2 \cdot 3600)^2} \cdot \frac{\rho_{gp}}{\rho_{lp} - \rho_{gp}} \quad (10)$$

$$Q_w = Q_p \cdot \left(\frac{L_w}{L_p}\right)^{\frac{5}{2}} \cdot \left(\frac{\rho_{gp}}{\rho_{gw}}\right)^{\frac{1}{2}} \cdot \left(\frac{\rho_{lw} - \rho_{gw}}{\rho_{lp} - \rho_{gp}}\right)^{\frac{1}{2}} \quad (11)$$

$$Q_w = Q_p \cdot \left(\frac{L_w}{L_p}\right)^{\frac{5}{2}} \cdot \left(\frac{\rho_{gp}}{\rho_{gw}}\right)^{\frac{1}{2}} \cdot \left(\frac{\rho_{lw}}{\rho_{lp}}\right)^{\frac{1}{2}} \quad (12)$$

where the subscripts w and p represent the water model and the prototype respectively; u is the bottom blowing gas velocity, m/s; g is the gravitational acceleration, m/s²; ρ is the density, kg/m³; L is the characteristic size, m; Q is the bottom blowing gas flow, Nm³/h; n is the number of bottom blowing components. Since the liquid density is much larger than the gas density, the effect of gas density is ignored in the fourth term on the right side of the Eq. 11. The bottom blowing gas flow rate for the hydraulics experiment and the prototype are shown in Table 2.

In the water model experiment, a saturated potassium chloride solution (generally 30 ml) was used as a tracer; two DJS-10C conductivity electrodes are arranged in an asymmetric position at the bottom of the furnace, to detect the change in conductivity of the molten pool, thereby obtaining a mixing time for the pool. In order to eliminate human error, each group of experiments was repeated three times, and the arithmetic mean was obtained.

B. Computation Validation

In order to verify the applicability of the model, during the numerical simulation process in Sect. 2, the same model was used as in the water model experiment. During the calculation, the tracer was added at the same position as that of the conductivity electrode in the water model. When the mole fraction of the tracer reached 95% of the final mole fraction, it was considered that this was the mixing moment.

Figure 5 shows the conductivity curve for the molten pool, with respect to the monitoring time, in the water model experiment of Scheme 4. It can be seen from the figure that the conductivity of the two electrodes is equal before the addition of the tracer, this is consistent with the fluid continuity characteristics. When the tracer was added, the conductivity at that point increases. As time passes, the conductivity again becomes equal. For this study, when the difference between the two conductivity curves is less than 5%, the moment of mixing is considered to have been reached. Figure 6 shows the tracer mole fraction curve during the numerical simulation of the water model. It can be seen from the figure that the mole fraction at the detection point gradually decreases with time, it is considered that when the difference between the two mole fraction curves is less than 5%, the mixing time is reached.

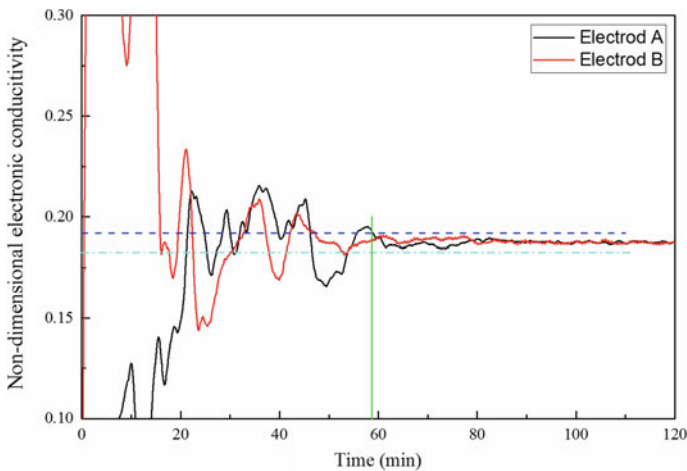


Fig. 5 The electronic conductivity change in the water model experiment (scheme 4)

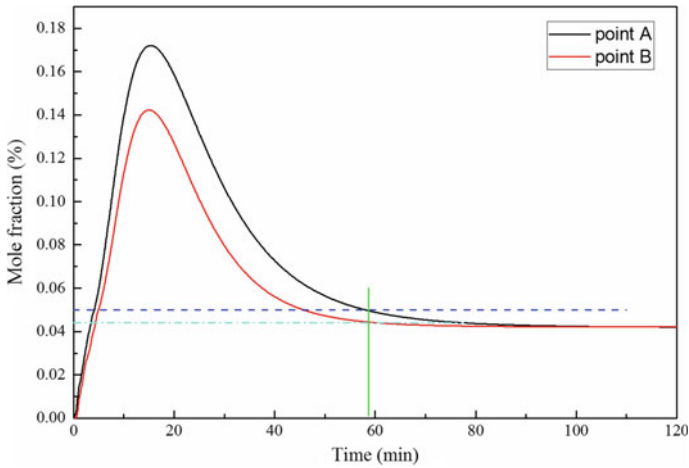


Fig. 6 The tracer mole fraction change in the numerical simulation (scheme 4)

Table 4 The mixing time of pool under water model experiment and numerical simulation

Item	The bottom blowing gas flow rate	Scheme			
		1	2	3	4
Water model experiment (s)	600	82.3	78.2	74.7	72.8
	800	67.4	63.3	60.5	58.7
	1000	62.9	57.9	56.2	55.7
Numerical simulation (s)	600	84.1	75.3	79.4	74.2
	800	70.9	66.9	59.5	58.3
	1000	63.5	56.5	56.8	55.8

Table 4 shows the mixing times for the water model experiment and the numerical simulation. It can be seen from the table that the maximum absolute error of the mixing time is less than 6.4%. Therefore, it can be considered that the model selected for the numerical simulation process is applicable.

Results and Discussion

A. Analysis of the Water Model Experiment

For the hydraulic experiment of the steelmaking process, the mixing time of the molten pool is an important evaluation index for the experimental scheme.

It can be seen from Fig. 7 that while increasing the bottom blowing flow rate

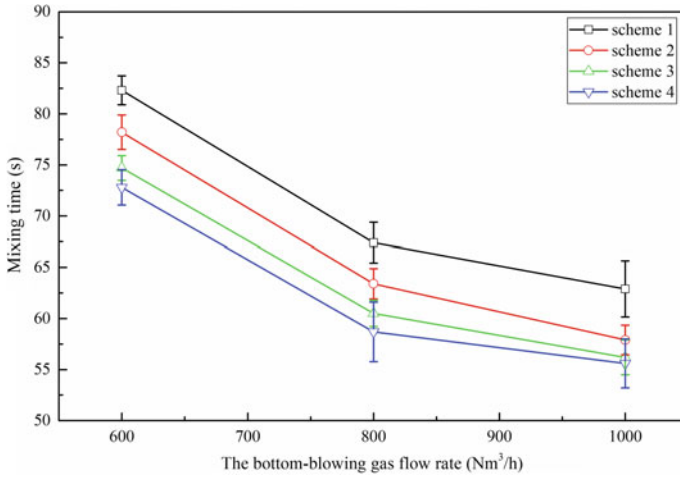


Fig. 7 The mixing time of water model experiments

from 600 Nm³/h to 1000 Nm³/h, the mixing time is gradually reduced and the amplitude decrease gradually slows down. The mixing time of the molten pool, in each experimental scheme, is positively correlated with the angle of the bottom blowing element.

B. Analysis of the Numerical Simulation

In this study, the influence of the angle of the bottom blowing element, on the dynamic characteristics of the molten pool is studied by numerical simulation. Figures 8 and 9 show velocity distribution diagrams of the longitudinal section of the molten pool and the cross sections at different depths, with different colors representing different speeds. Red represents a high-speed zone and blue represents a low-speed zone. According to the results of the water model experiment, and in the literature, when the bottom blowing flow rate is increased, it improves the stirring of the molten pool.

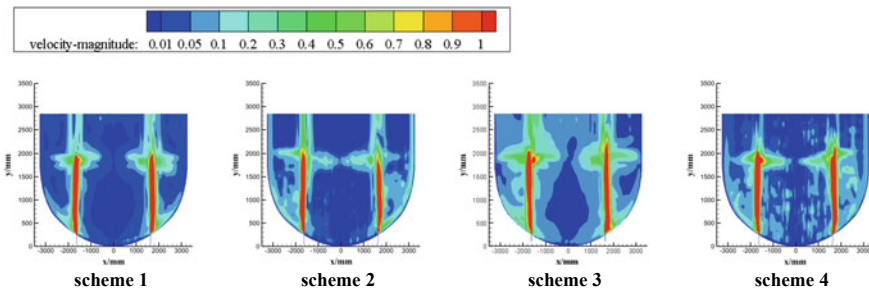


Fig. 8 Velocity distribution on longitudinal section in the molten pool

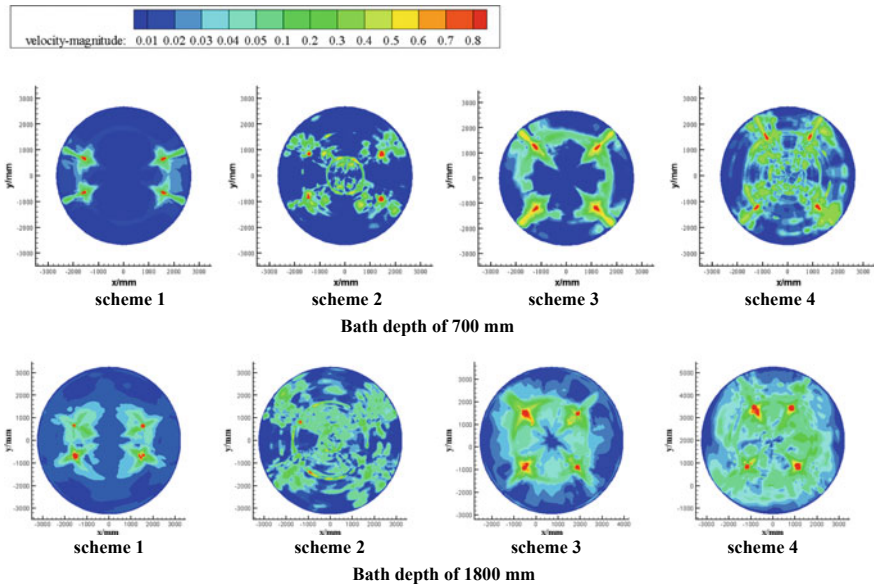


Fig. 9 Velocity distribution at the cross section of the molten pool

Therefore, the following discussion focuses on the numerical simulation results when the bottom blowing flow rate is $800 \text{ Nm}^3/\text{h}$, because it is an intermediate speed value.

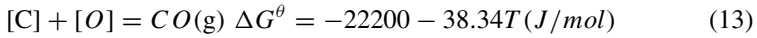
It can be seen from Fig. 8 that the low velocity zone in the molten pool is mainly distributed between the central region and near the furnace wall region. The velocity of the molten pool, near the bottom blow stream, is relatively large. As the angle is increased, the uniformity of the velocity distribution in the molten pool gradually increases.

It can be seen from Fig. 9, that as the depth of the molten pool increases, the uniformity of the velocity distribution increases. The reason for this is that the volume gradually expands during the ascending of the bottom blowing gas, therefore the kinetic energy is gradually transferred to the molten pool, and the velocity of the molten bath gradually increases. For a constant molten pool depth, as the angle between the bottom blowing elements increases, the velocity of the molten pool gradually increases. At the same time, the distribution area of the low velocity region in the molten pool gradually decreases. It can be seen that the center and the near wall, low velocity regions, in Scheme 1, are gradually reduced to the near wall area in Scheme 4. This feature correlates well with the position of the dead zone in the water simulation process.

C. Chemical Reactions in the Molten Bath

1. Decarburization efficiency and endpoint carbon–oxygen equilibrium

For converter steelmaking, the decarburization reaction is the central subject of research. The main reaction formula is Eq. 13.



$$K_c = \frac{p_{CO}}{a_{[C]} \cdot a_{[O]}} = \frac{p_{CO}}{f_C [%C] f_O [%O]} \tag{14}$$

Equation 14 is the reaction equilibrium constant of Eq. 13, where p_{CO} is the partial pressure of carbon monoxide, generally taken as 1 atm; $a_{[C]}$ and $a_{[O]}$ are the activity of carbon and oxygen, respectively, in molten steel, f_c and f_o are the activity coefficients of carbon and oxygen, [%C] and [%O] are the mass percentages of carbon and oxygen in molten steel. For the end-point molten steel, the carbon content is relatively low, so f_c and f_o are both 1, therefore Eq. 14 can be simplified to Eq. 15.

$$K_c = \frac{1}{[%C][%O]} \tag{15}$$

According to the physicochemical principle, the Gibbs free energy analysis of Eq. 14 can be obtained from Eq. 16. It is observed that the product of the carbon and oxygen mass fraction in the molten steel is only related to temperature, and $m = [%C][%O]$ is defined as the carbon and oxygen concentration of molten steel.

$$\lg([%C][%O]) = -\frac{1160}{T} - 2.003 \tag{16}$$

The tapping temperature of the converter is generally around 1873 K. When $p_{CO} = 1$ atm, the content of carbon–oxygen equilibrium in the molten steel is 0.0024.

In the industrial experiment process, a total of 3282 test data were taken for the entire furnace campaign. The distribution of the scatter plots is shown in Fig. 10. It

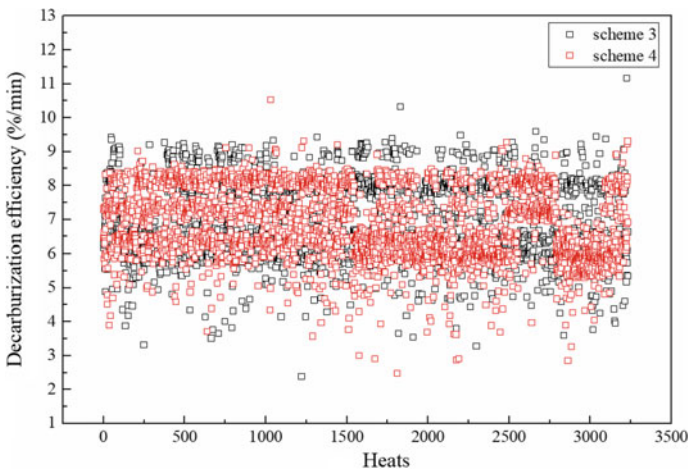
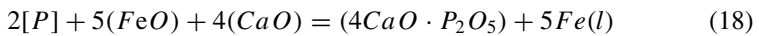
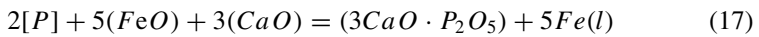


Fig. 10 Distribution of decarburization efficiency in the molten pool

can be seen that the distribution of carbon–oxygen equilibrium in the steel sample, at the end of Scheme 4, was lower than that in Scheme 3; Fig. 11 is an average of the test data. It was found that the content of carbon–oxygen equilibrium in Scheme 4 was 9.52% lower than in Scheme 3. From this result, it can be seen that the stirring of the molten pool, at the bottom of Scheme 4, is better than that shown in Scheme 3.

2. Dephosphorization effect

Phosphorus in molten steel can cause a cold and brittle phenomenon. Therefore, the dephosphorization reaction is important in the steelmaking process. In the actual production process, the dephosphorization reaction is carried out by using calcium oxide, the reaction formula is shown in Eqs. 17, 18 and 19 is a simplified equation of the dephosphorization reaction.



$$2[P] + 5[O] = (P_2O_5) \lg K_P = \frac{a_{(P_2O_5)}}{[\%P]^2 [\%O]^5} = \frac{36850}{T} - 29.07 \tag{19}$$

The dephosphorization reaction is a typical slag-steel reaction. Under the condition of certain bath temperature and alkalinity, a good kinetic performance of the molten pool increases the mass transfer rate of the elements in the molten steel. In the industrial test process, a total of 1992 samples were taken for the dephosphorization rate, and the average value distribution is shown in Fig. 12. It can be seen from the industrial experimental results that the dephosphorization rate of Scheme 4 is 1.06 times that of Scheme 3. This conclusion indicates that the mass transfer rate of the elements in the molten pool of Scheme 4 is faster than that of Scheme 3, and thus is favorable to the reaction of the slag steel in the furnace.

Fig. 11 Average endpoint carbon–oxygen equilibrium of scheme 3 and scheme 4

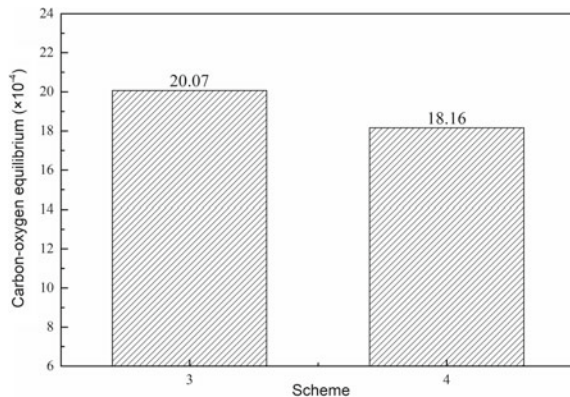
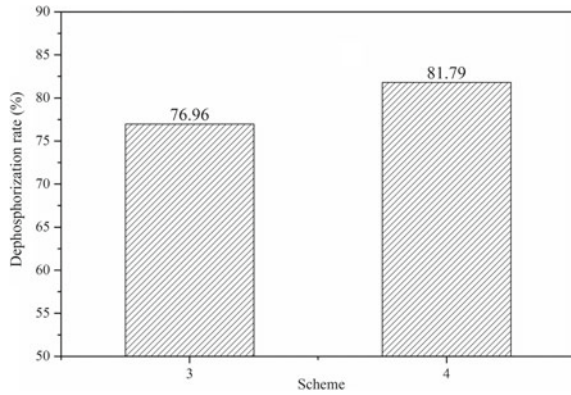
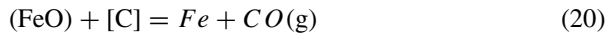


Fig. 12 Average dephosphorization rate of scheme 3 and scheme 4



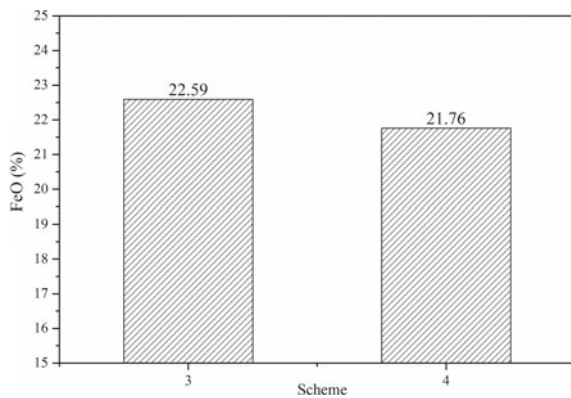
Endpoint Slag Composition

The slagging regime has a huge impact on steelmaking. The FeO has a great influence on the consumption of steel materials, the utilization rate of alloys, and the refining process. However, due to the kinetic conditions of the molten pool, a part of FeO still exists in the slag. The higher the FeO content in the slag, the greater the consumption of the steel material.



It can be seen that the molten pool dynamic conditions have a significant impact on the control of FeO content, under certain conditions of the top blowing process. In the industrial experiment, 1777 sampling samples were taken and analyzed. The results are shown in Fig. 13. The FeO content in Scheme 4 is reduced by 3.67% more than in Scheme 3. This conclusion is in good agreement with both the numerical and water simulation results.

Fig. 13 Content of FeO of scheme 3 and scheme 4 in endpoint slag



Conclusions

This study has established a 300t converter experimental water model, a three-dimensional numerical simulation model, and industrial experiments have been conducted. The influence of the bottom blowing stream, on the dynamic characteristics and chemical reactions in the molten pool, under different angles of bottom blowing elements, is studied.

The mathematical model applied in the numerical simulation process shows good consistency with the experimental results from the water model. With an increase in the angle between the bottom blowing elements, the stirring ability of the bottom blowing stream on the molten pool is enhanced. This conclusion is clearly verified in both the numerical simulation and water simulation process. With an increase in the angle between the bottom blowing elements, the carbon and oxygen concentration, FeO, dephosphorization rate and other indicators of impurities in the actual production process, show a decreasing trend. The results from the production process experiments not only correlate well with the results of the water model experiment, but also show a good level of consistency with the numerical simulation results.

References

1. Zhang MY, Sun XK, Wang GD, Liu XH, Zhang MH (2000) Current conditions and development of application of mathematical simulation technology in China's iron and steel industry. *Res Iron Steel* 3:53–58
2. Liu AH, Li Q, Feng MX, Zou ZS (2003) Water modeling of optimizing blowing technical parameters in LBE. *J Mater Metall* 2(1):21–24
3. Choudhary SK, Ajmani SK (2006) Evaluation of bottom stirring system in BOF steelmaking vessel using cold model study and thermodynamic analysis. *ISIJ Int* 46(8):1171–1176
4. Chen R, Luo ZG, Yang CG, Zou ZS (2008) A study of water model on size and space distribution of slag dispersed phase on combined blowing of converter. *Special Steel* 1:13–15
5. Lou WT, Li Y, Zhu MY (2011) Numerical simulation of gas-liquid two-phase popularity in top-bottom combined blowing converter. *Chin J Process Eng* 11(6):926–932
6. Liu F, Zhu R, Dong K, Bao X, Fan SL (2015) Simulation and application of bottom-blowing in electrical arc furnace steelmaking process. *ISIJ Int* 55(11):2365–2373
7. Luomala Matti J, Fabritius Timo MJ, Härkki Jouko J (2004) The effect of bottom nozzle configuration on the bath behavior in the BOF. *ISIJ Int* 44(5):809–816
8. Lai ZY, Xie Z, Zhong LC (2008) Influence of bottom tuyere configuration on bath stirring in a top and bottom combined blown converter. *ISIJ Int* 48(6):793–798
9. Gu L, Irons GA (2001) Physical and mathematical modeling of bottom stirring and gas evolution in electric arc furnaces. *Iron Steelmak* 28(1):57–68
10. Hirt CW, Nichols BD (1981) Volume of fraction (VOF) method for the dynamics of free boundary. *J Comput Phys* 39:201–225
11. Launder BE, Spalding DB (1972) *Lectures in mathematical model of turbulence*. Academic Press, London